Article

Uranyl Functionalization Mediated by Redox-Active Ligands: Generation of O-C Bonds via Acylation

Ezra J. Coughlin, Yusen Qiao, Ekaterina Lapsheva, Matthias Zeller, Eric J. Schelter, and Suzanne C. Bart

J. Am. Chem. Soc., **Just Accepted Manuscript** • Publication Date (Web): 11 Dec 2018

Uranyl Functionalization Mediated by Redox-Active Ligands: Generation of O-C Bonds *via* Acylation

*Ezra J. Coughlin†, Yusen Qiao‡, Ekaterina Lapsheva‡, Matthias Zeller†, Eric J. Schelter‡ and Suzanne C. Bart†**

† Department of Chemistry, Purdue University, West Lafayette, Indiana 47901, USA

‡ P. Roy and Diana T. Vagelos Laboratories, Department of Chemistry, University of Pennsylvania, 231 South 34th Street, Philadelphia, Pennsylvania 19104, USA.

Abstract: A series of uranyl compounds with the redox-active iminoquinone ligand have been synthesized and their electronic structure elucidated using multinuclear NMR, EPR, electronic absorption spectroscopies, SQUID magnetometry, and X-ray crystallography. Characterization and analysis of the iminoquinone (iq^0) complex, (^{dipp}iq)$UO_2(OTf)_2THF$ (**1-iq**), the iminosemiquinone (isq^{1-}) complex, ($^{dipp}isq)_2UO_2THF$ (**2-isq**), and the amidophenolate (ap^{2-}) complex, [($^{dipp}ap)_2UO_2THF$][K(18-crown-6)$(THF)_2$]$_2$ (**3-ap crown**) show that reduction events are ligand-based, with the uranium center remaining in the hexavalent state. Reactivity of **2-isq** with B-chlorocatecholborane or pivaloyl chloride leads to U-O_{uranyl} bond scission and reduction of U(VI) to U(IV) concomitant with ligand oxidation along with organic byproducts. ^{18}O isotopic labeling

experiments along with IR spectroscopy, mass spectrometry, and multinuclear NMR spectroscopy confirm the organic byproducts contain oxygen atoms which originate from U-O_{uranyl} bond activation.

Introduction

The uranyl ion, $[UO_2]^{2+}$, is the most recognizable actinide containing species due to its prevalence in aqueous environments and in the solid state.[1] Characterized by its robust *trans*-oxo ligands and +6 oxidation state, derivatives of this ion form naturally from interactions of water with uranium ore deposits, as well as anthropogenically from depleted uranium targets,[2] nuclear waste streams,[3] and uranium mining.[4] The high solubility of this ion in water is problematic as its increased mobility in this form causes environmental contamination. In anaerobic environments, uranyl can be reduced to its +5 (unstable) and +4 (stable) forms, greatly reducing its water solubility and facilitating removal from the environment.[5]

The persistence of uranyl is attributed to its strong uranium-oxygen bonds, which are not easily functionalized or cleaved. Taking inspiration from Nature, recent work in non-aqueous uranyl chemistry has demonstrated that transformation of U-O_{uranyl} bonds may be facilitated by reduction events to generate U(IV) ions, in which pentavalent intermediates are likely involved. One strategy, demonstrated by Duval and co-workers, involves the photochemical reduction of hexavalent $[UO_2(dppmo)_2(OPPh_3)][\ OTf]_2$ (dppmo = $Ph_2P(O)CH_2P(O)Ph_2$) in the presence of BF_4^-

anions, producing the corresponding uranium(IV) difluoride species.[6] Reductive silylation of the uranyl ion has also been studied[7-13] and optimized,[7] while strongly Lewis acidic titanium[14] and borane[15] compounds have also proven to be potent reductants for the generation of uranium (IV) *via* U-O_{uranyl} bond activation. P. Arnold and co-workers have pioneered the use of a specialized dipyrrin ligand and strongly Lewis acidic atoms to facilitate uranyl functionalization by shifting the U(V) – U(IV) reduction into an accessible redox range. More recently, work from their lab has also demonstrated reduction of the terminal oxos in uranyl using silanes or boranes.[16] In each case, the corresponding silyl and boryl ethers are released, showing full U-O_{uranyl} bond scission.

Our group has reported the utility of redox-active ligands in uranyl functionalization and U-O_{uranyl} bond scission as well. Treating Cp*UO_2(^{Mes}PDI^{Me}) (Cp* = 1,2,3,4,5-pentamethylcyclopentadienide; ^{Mes}PDI^{Me} = 2,6-((Mes)N=CMe)$_2$-C_5H_3N; Mes = 2,4,6-trimethylphenyl), which contains a singly reduced pyridine(diimine) ligand and a hexavalent uranyl ion, with stoichiometric equivalents of Me_3SiI results in stepwise oxo silylation to form tetravalent $(Me_3SiO)_2UI_2$(^{Mes}PDI^{Me}).[17] Additional equivalents of Me_3SiI results in full uranium-oxo bond cleavage and the formation of UI_4(1,4-dioxane)$_2$ with extrusion of hexamethyldisiloxane. The necessary electron equivalents derive from the reduced pyridine(diimine) ligand and loss of the Cp* ring in this example.

Much of the work in uranyl functionalization is based on silylation and borylation of U-O_{uranyl} bonds, with formation of O-Si and O-B bonds acting as a strong

thermodynamic driving force. Currently, there are no examples of transformations of U-O_{uranyl} bonds where O-C bonds are formed. We hypothesized that U-O_{uranyl} bonds could undergo such a conversion with electrophilic carbon-containing substrates when mediated by reduced redox-active ligands. The iminoquinone family would be effective for such a task, as this ligand set has mediated multi-electron reactions with low-valent metals[18-23] and would obviate the need for an external reductant by its ability to exist in a reduced state (Figure 1). The most oxidized form of this ligand, the iminoquinone (iq^0), can be reduced to the iminosemiquinone (isq^{1-}), which is characterized by a ligand radical. Further reduction results in the formation of the amidophenolate ligand (ap^{2-}), which stores two electrons in its π^* orbitals.[24]

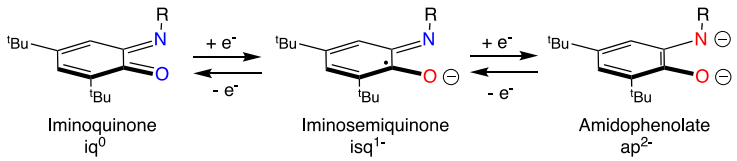

Figure 1. Redox chemistry demonstrated by the iminoquinone/amidophenolate ligand. Red atoms denote anionic bonds, while blue atoms engage in dative (neutral) bonding.

Herein, we report a new series of uranyl derivatives containing redox-active iminoquinone/amidophenolate ligands. Storing electrons in this ligand framework generates uranyl complexes with unprecedented electronic structures, including an unusual diradical species. These ligands facilitate multi-electron chemistry at uranyl centers, allowing the complete functionalization and removal of the robust *trans*-oxo ligands through borylation and acylation reactions. Full spectroscopic, structural, and

magnetic characterization is provided, as well as isotopic labeling experiments to highlight the transformation of the uranyl moiety.

Experimental Section

General Considerations. All air- and moisture-sensitive manipulations were performed using standard Schlenk techniques or in an MBraun inert atmosphere drybox with an atmosphere of purified nitrogen. The MBraun drybox was equipped with a cold well used for freezing samples in liquid nitrogen as well as two -35 °C freezers for cooling samples and crystallizations. Solvents for sensitive manipulations were dried and deoxygenated using literature procedures with a Seca solvent purification system.[25] Water (^{18}O, 97%) was purchased from Cambridge Isotope Laboratories and used as received. Benzene-d_6 was purchased from Cambridge Isotope Laboratories, dried with molecular sieves and sodium and degassed by three freeze–pump–thaw cycles. Chloroform-*d* and pyridine-d_5 were purchased from Cambridge Isotope Laboratories, dried with molecular sieves, and degassed by three freeze–pump–thaw cycles. 4,6-di-*tert*-butyl-2-[(2,6-diisopropylphenyl)imino]quinone (^{dipp}iq)[23], potassium graphite (KC_8)[26], uranyl dichloride ($[UO_2Cl_2(THF)_2]_2$)[27], uranyl triflate $UO_2(OTf)_2(THF)_3$[28], and uranium tetrachloride (UCl_4)[29] were prepared according to literature procedures. 18-crown-6 (18-C-6) and B-chlorocatecholborane (Cl-BCat) were purchased from Sigma Aldrich and dried under vacuum on a Schlenk line overnight prior to use. Pivaloyl chloride (Piv-Cl) was purchased from Sigma Aldrich, degassed by three freeze–pump–thaw cycles, and dried with molecular sieves prior to use.

^{1}H NMR spectra were recorded on a Varian Inova 300 or Bruker AV-III-400-HD spectrometer operating at 299.99 and 400.13 MHz, respectively. All chemical shifts are reported relative to the peak for $SiMe_4$, using ^{1}H (residual) chemical shifts of the solvent as a secondary standard. $^{13}C\{^{1}H\}$ NMR spectra were recorded on a Bruker AV-III-HD spectrometer operating at 100.61 MHz. ^{19}F NMR spectra were recorded on a Bruker AV-III-HD spectrometer operating at 376.50 MHz. ^{11}B NMR spectra were recorded on a Varian Inova 300 spectrometer operating at a frequency of 96.24 MHz. ^{11}B chemical shifts are reported relative to the peak for $BF_3 \bullet Et_2O$ (0.0 ppm). The spectra for all paramagnetic molecules were obtained by using an acquisition time of 0.5 s, thus, the peak widths reported have an error of ±2 Hz. For all paramagnetic molecules, the ^{1}H NMR data are reported with the chemical shift, followed by the peak width at half height in Hz, the integration value, and, where possible, the peak assignment. All voltammetric data were obtained under inert atmosphere conditions using external electrical ports of the MBraun inert drybox. All data were obtained using a Gamry Instruments Interface 1000 model potentiostat using the Gamry Instruments Laboratory software. All data were collected on samples in THF with 0.1 M $[Bu_4N][PF_6]$ supporting electrolyte concentration, and using an internal resistance compensation of approximately 2000 ohms. Solutions were analyzed in 10 mL beakers, with a 3 mm glassy carbon working electrode, a Pt wire counter electrode, and an Ag wire quasi-reference electrode. Potential corrections were performed at the end of the experiment using the Fc/Fc^{+} couple as an internal standard. X-Band EPR spectra were recorded on a Bruker EMX EPR spectrometer and simulated using the EasySpin toolbox in

MATLAB. Electronic absorption measurements were recorded at 294 K in THF in sealed, 1 cm quartz cuvettes with a Cary 6000i UV-vis-NIR spectrophotometer. Elemental analyses were performed by Midwest Microlab (Indianapolis, IN). Solid state infrared spectra were recorded using a Thermo Nicolet 6700 spectrophotometer.

Synthesis of (^{dipp}iq)$UO_2(OTf)_2$THF (1-iq). A 20-mL scintillation vial was charged with $UO_2(OTf)_2(THF)_3$ (0.100 g, 0.176 mmol) and 5 mL diethyl ether. A separate 20-mL scintillation vial was charged with ^{dipp}iq (0.067 g, 0.176 mmol), dissolved in 5 mL diethyl ether and added dropwise to the stirring $UO_2(OTf)_2(THF)_3$ slurry. A reddish-brown solution was observed. After 6 hours, the volatiles were removed *in vacuo*. The resulting reddish-purple solid was washed with cold diethyl ether (3 × 10 mL) to afford a red powder (0.106 g, 0.132 mmol, 75% yield) assigned as **1-iq**. X-ray quality crystals were obtained from a concentrated toluene solution stored at -35 °C. Elemental analysis of $C_{32}H_{45}NO_{10}F_6S_2U$: Calculated, C, 37.69; H, 4.45; N, 1.37. Found, C, 38.07; H, 4.80; N, 1.29. ^{1}H NMR (C_6D_6, 300MHz, 25 °C): δ = 0.64 (s, 9H, C(CH_3)$_3$), 0.84 (d, 7, 6H, CH(CH_3)$_2$), 1.21 (d, 7, 6H, CH(CH_3)$_2$), 1.44 (s, 9H, C(CH_3)$_3$), 1.93 (br s, 4H, THF), 2.70 (sept, 7, 2H, C*H*(CH$_3$)$_2$), 5.26 (br s, 4H, THF), 6.17 (d, 2, 1H, C*H*), 7.28 (d, 2, 1H, C*H*), 7.31 (s, 2H, C*H*), 7.28 (s, 1H, C*H*). ^{1}H NMR ($CDCl_3$, 400 MHz, 25 °C): δ = 1.03 (d, 6.8, 6H, CH(CH_3)$_2$), 1.04 (d, 6.8, 6H, CH(CH_3)$_2$), 1.19 (s, 9H, C(CH_3)$_3$), 1.72 (s, 9H, C(CH_3)$_3$), 2.46 (br s, 4H, THF), 2.53 (sept, 6.8, 2H, C*H*(CH$_3$)$_2$), 5.21 (br s, 4H, THF), 6.21 (s, 1H, C*H*), 7.45 (d, 7.7, 2H, C*H*), 7.53 (t, 7.7, 2H, C*H*), 7.28 (s, 1H, C*H*). ^{13}C{^{1}H} NMR ($CDCl_3$, 100 MHz, 25 °C): δ = 22.66, 24.99, 26.35, 27.89, 29.10, 36.16, 36.50, 116.36, 124.85, 129.64, 138.11,

143.90, 145.39, 150.40, 160.90, 169.15, 195.99. ^{19}F NMR ($CDCl_3$, 376.5 MHz, 25 °C): δ = -78.10.

Synthesis of (^{dipp}isq)$_2$UO$_2$THF (2-isq). A 20-mL scintillation vial was charged with $[UO_2Cl_2(THF)_2]_2$ (0.100 g, 0.103 mmol) and 5 mL THF. A separate 20-mL scintillation vial was charged with ^{dipp}iq (0.156 g, 0.412 mmol), dissolved in 5 mL THF and added dropwise to the stirring $[UO_2Cl_2(THF)_2]_2$ slurry. After stirring for 15 minutes, KC_8 (0.056 g, 0.412 mmol) was weighed by difference and added over 5 minutes, resulting in a rapid color change from red to dark green. After 2 hours, the slurry was filtered through Celite and volatiles were removed *in vacuo*. The remaining mixture was recrystallized from *n*-pentane to afford a green powder (0.152 g, 0.138 mmol, 67% yield) assigned as **2-isq**. Single, X-ray quality crystals were obtained from a concentrated diethyl ether solution at -35 °C. Elemental analysis of $C_{56}H_{82}N_2O_5U$: Calculated, C, 61.07; H, 7.51; N, 2.54. Found, C, 60.94; H, 7.70; N, 2.22. ^{1}H NMR (C_6D_6, 300MHz, 25 °C): δ = 0.05 (br s), 1.50 (br s), 2.47 (br s), 3.68 (br s), 3.89 (br s), 6.86 (br s), 7.70 (br s), 16.47 (br s), 53.64 (br s).

Synthesis of [[(^{dipp}ap)$_2$U][K(THF)$_2$]$_2$]$_2$ (3-ap) from 2-isq. A 20-mL scintillation vial was charged with **2-isq** (0.100 g, 0.091 mmol) and 10 mL THF. While stirring, KC_8 (0.025 g, 0.181 mmol) was weighed by difference and added over 5 minutes, resulting in a rapid color change from dark green to black. After 1 hour, the solution was filtered through Celite and volatiles were removed *in vacuo*. The crude mixture was washed with 10 mL cold *n*-pentane to afford a tan powder (0.140 g, 0.056 mmol, 62% yield) assigned as **3-ap**. Single, X-ray quality crystals were obtained from a concentrated diethyl ether solution

at -35 °C. Elemental analysis of $C_{120}H_{180}N_4O_{12}K_4U_2$: Calculated, C, 57.58; H, 7.25; N, 2.24. Found, C, 57.84; H, 7.34; N, 2.34. ^{1}H NMR (NC_5D_5, 300MHz, 25 °C): δ = 0.82 (d, 7, 12H, CH(CH_3)$_2$), 1.29 (d, 7, 12H, CH(CH_3)$_2$), 1.40 (s, 18H, C(CH_3)$_3$), 1.83 (s, 18H, C(CH_3)$_3$), 4.37 (sept, 7, 4H, C*H*(CH$_3$)$_2$), 5.73 (s, 2H, C*H*), 6.49 (s, 2H, C*H*), 6.80 (t, 8, 2H, C*H*), 7.02 (d, 8, 4H, C*H*). ^{13}C{^{1}H} NMR (NC_5D_5, 100 MHz, 25 °C): δ = 23.28, 25.48, 26.20, 26.95, 30.80, 32.39, 34.26, 34.81, 67.50, 107.69, 110.48, 122.19, 122.78, 130.77, 137.50, 148.31, 154.09, 156.96.

Synthesis of [(^{dipp}ap)$_2$UO$_2$THF][K(18-crown-6)(THF)$_2$]$_2$ (3-ap crown) from 3-ap. A 20-mL scintillation vial was charged with **3-ap** (0.100 g, 0.040 mmol) and 5 mL THF. While stirring, 18-crown-6 (0.042 g, 0.160 mmol) was weighed by difference and added. After 1 hour, volatiles were removed *in vacuo*. The crude mixture was washed with 10 mL cold diethyl ether to afford a white powder (0.121 g, 0.061 mmol, 76% yield) assigned as **3-ap crown**. Single, X-ray quality crystals were obtained from a concentrated THF/toluene (1:1) solution stored at -35 °C. Elemental analysis of $C_{96}H_{162}N_2O_{21}K_2U$: Calculated, C, 57.75; H, 8.18; N, 1.40. Found, C, 57.27; H, 8.07; N, 2.14. The EA values for C and N are off by more than 0.4%, which may be an indication of decomposition as a result of the reactive nature of this complex. ^{1}H NMR (NC_5D_5, 300MHz, 25 °C): δ = 1.24 (d, 7, 12H, CH(CH_3)$_2$), 1.37 (d, 7, 12H, CH(CH_3)$_2$), 1.44 (s, 18H, C(CH_3)$_3$), 1.55 (s, 18H, C(CH_3)$_3$), 3.43 (s, 24H, CH_2), 4.87 (sept, 7, 4H, C*H*(CH$_3$)$_2$), 5.90 (d, 2, 2H, C*H*), 6.56 (d, 3, 2H, C*H*), 7.06 (t, 8, 2H, C*H*), 7.38 (d, 8, 4H, C*H*). ^{13}C{^{1}H} NMR (NC_5D_5, 100 MHz, 25 °C): δ = 23.74, 24.67, 25.49, 26.53, 26.90, 30.92, 31.33, 32.63, 33.94, 34.27, 34.96, 67.50, 70.08, 106.69, 108.35, 121.58, 122.64, 130.49, 135.82, 148.59, 153.97, 156.48, 159.31.

Synthesis of (^{dipp}iq)(^{dipp}isq)UO_2Cl (4-iq/isq). A 20-mL scintillation vial was charged with $[UO_2Cl_2(THF)_2]_2$ (0.275 g, 0.283 mmol) and 8 mL THF. A separate 20-mL scintillation vial was charged with ^{dipp}iq (0.430 g, 1.133 mmol), dissolved in 10 mL THF and added dropwise to the stirring $[UO_2Cl_2(THF)_2]_2$ slurry. After stirring for 15 minutes, KC_8 (0.077 g, 0.567 mmol) was weighed by difference and added over 5 minutes, resulting in a rapid color change from red to brown. After 2 hours, the slurry was filtered through Celite and volatiles were removed *in vacuo*. The brown solid was triturated with diethyl ether (2 × 10 mL) and *n*-pentane (2 × 10 mL) then dried *in vacuo*. The resulting black powder was washed with cold *n*-pentane (3 × 10 mL) to afford a greenish brown powder (0.400 g, 0.376 mmol, 66% yield) assigned as **4-iq/isq**. Single, X-ray quality crystals were obtained from a concentrated diethyl ether solution at -35 °C. Elemental analysis of $C_{52}H_{74}N_2O_4ClU$: Calculated, C, 58.66; H, 7.01; N, 2.63. Found, C, 58.91; H, 7.13; N, 2.53. ^{1}H NMR (C_6D_6, 300MHz, 25 °C): δ = 2.09 (br s), 3.10 (br s), 4.90 (br s).

Reaction of 2-isq with 4 eq. Cl-BCat. A 20-mL scintillation vial was charged with **2-isq** (0.100 g, 0.091 mmol) and 10 mL of THF. The vial was placed in the coldwell and the solution was frozen. Upon thawing, Cl-BCat (0.056 g, 0.363 mmol) was weighed by difference and added to the stirring solution. After warming to room temperature for 1 hour, volatiles were removed *in vacuo*. The products of the reaction were identified to be UCl_4(^{dipp}iq$_2$)$(THF)_2$ and $BOBCat_2$ by ^{1}H and ^{11}B NMR. The reaction mixture was washed with cold *n*-pentane (2 × 5 mL) to separate organics from the uranium product, producing a black powder (0.057 g, 0.063 mmol, 69% yield).

Independent synthesis of ^{dipp}iqUCl$_4$(THF)$_2$ (5-iq). A 20-mL scintillation vial was charged with UCl_4 (0.100 g, 0.263 mmol) and 10 mL THF. In a separate vial, ^{dipp}iq (0.100 g, 0.263 mmol) was dissolved in 5 mL of THF and added dropwise to the stirring UCl_4 solution. The solution immediately changed color from green to black. After 8 hours the solvent was removed *in vacuo* and washed with *n*-pentane (2 × 5 mL) to yield a black powder (0.184 g, 242 mmol, 92% yield). This sample was submitted for elemental analysis. Single, X-ray quality crystals were obtained from a concentrated THF solution at -35 °C. Elemental analysis of $C_{26}H_{37}N_1O_1Cl_4U$ (solvent free): Calculated, C, 41.12; H, 4.91; N, 1.84. Found, C, 40.83; H, 5.02; N, 1.64. ^{1}H NMR (C_6D_6, 300MHz, 25 °C): δ = -14.89 (4, 1H, C*H*), -6.49 (3, 9H, C(CH_3)$_3$), -5.16 (103, 3H, CH(CH_3)), -5.07 (35, 4H, THF), -3.79 (106, 3H, CH(CH_3)),-3.61 (35, 4H, THF), -1.07 (4, 9H, C(CH_3)$_3$), -0.54 (4, 1H, C*H*), 1.98 (32, 2H, C*H*), 9.11 (t, *J* = 7 Hz, 1H, C*H*), 10.87 (37, 4H, THF), 11.65 (36, 4H, THF), 12.29 (115, 3H, CH(CH_3)), 13.99 (118, 3H, CH(CH_3)), 19.44 (10, 2H, C*H*).

Reaction of 2-isq with 4 eq. Piv-Cl. A 20-mL scintillation vial was charged with **2-isq** (0.080 g, 0.073 mmol), dissolved in 10 mL benzene and transferred to a 25 mL receiving flask. Pivaloyl chloride (0.035 g, 0.290 mmol) was weighed by difference and added to the green, stirring solution. The flask was sealed and then heated to 50 °C for 8 hours, producing a red solution. After cooling to room temperature for 1 hour, volatiles were removed *in vacuo*. The products of the reaction were identified by ^{1}H NMR to be pivaloyl anhydride, and **6-iq**. The reaction mixture was washed with cold *n*-pentane (2 × 5 mL) to separate organics from the uranium product, producing a brown powder (0.061 g, 0.053 mmol, 73% yield).

Independent synthesis of $^{dipp}iq_2UCl_4$ (6-iq). A 20-mL vial was charged with UCl_4 (0.056 g, 0.142 mmol) and 8 mL benzene. In a separate vial, ^{dipp}iq (0.119 g, 0.312 mmol) was dissolved in benzene (8 mL) and added dropwise to the stirring UCl_4 slurry. The reddish-brown mixture was then transferred to a receiving flask, sealed, and heated to 50 °C for 16 hours. The solvent was removed *in vacuo* and the resulting brown powder washed with *n*-pentane (2 × 10 mL), leaving **6-iq** (0.144 g, 0.126 mmol, 89% yield). Elemental analysis of $C_{52}H_{74}N_2O_2Cl_4U$: Calculated, C, 54.83; H, 6.55; N, 2.46. Found, C, 55.64; H, 6.37; N, 2.59. ^{1}H NMR (C_6D_6, 300MHz, 25 °C): δ = -75.30 (19, 2H, C*H*), -5.66 (t, *J* = 7 Hz, 2H, C*H*), -2.36 (12, 18H, C(CH_3)$_3$), 7.03 (8, 12H, CH(CH_3)$_2$), 7.25 (8, 2H, C*H*), 8.81 (10, 12H, CH(CH_3)$_2$), 19.07 (7, 18H, C(CH_3)$_3$), 28.96 (27, 4H, C*H*(CH$_3$)$_2$), 56.68 (d, *J* = 7 Hz, 4H, C*H*).

Synthesis of ^{18}O-Labeled $[UO_2Cl_2(THF)_2]_2$. This procedure was developed by adapting literature procedures.[27, 30] A 25-mL, borosilicate glass Schlenk flask was charged with approximately 1 g of $UO_2Cl_2(H_2O)_x$ (x = 1-3) and purged with argon. Against a flow of argon, 1 mL of $H_2{}^{18}O$ was added via pipette. After 1 minute of purging with argon, the flask was sealed. The yellow solution was gently stirred in front of a UV lamp (365 nm). *Note, using $[UO_2Cl_2(THF)_2]_2$ as the uranium source leads to decomposition of the material, as evidenced by color change from yellow to green and precipitation*. After 12 days, the water was removed from the yellow slurry *in vacuo*, yielding a yellow powder. From this material, anhydrous ^{18}O-labeled $[UO_2Cl_2(THF)_2]_2$ was obtained via a previously published procedure.[27] IR spectroscopy was employed to confirm the incorporation of ^{18}O into the U-O_{uranyl} (Figure S20).

Results and Discussion

Synthesis and Characterization of Reduction Series. Initially, a neutral ^{dipp}iq U(VI) complex was synthesized to provide a baseline for studies of more reduced species and allow comparison of spectroscopic data. Ligation of uranyl triflate, $UO_2(OTf)_2(THF)_3$, was accomplished by stirring with an equimolar amount of ^{dipp}iq in diethyl ether (Eq. 1). Upon workup, a red-purple powder was obtained in good yield (76%). The ^{1}H NMR spectrum (Figure S1) displayed 9 resonances slightly shifted from those observed for the free ligand, indicative of binding to the diamagnetic, U(VI), f^0 ion. Two additional, broad resonances, assignable as one bound THF molecule, were also observed at 1.93 and 5.26 ppm.

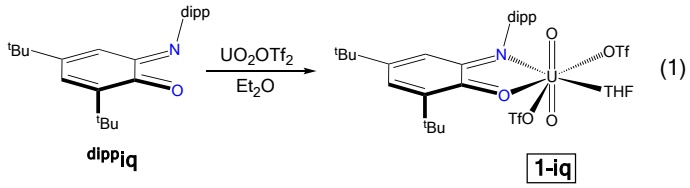

(1)

To unequivocally determine the number of coordinated ligands and examine the structural parameters of the complex, single crystals of **1-iq**, grown from toluene, were analyzed using X-ray diffraction. Refinement of the data revealed a seven-coordinate pentagonal bipyramidal uranyl coordination complex with one ^{dipp}iq ligand, one THF molecule, and two bound triflate anions in the equatorial plane along with the oxo ligands in axial positions (Figure 2, left; Table 1). The U-O_{uranyl} distance of 1.745(5) Å and O_{uranyl}-U-O_{uranyl} angle of 179.1(2)° are as expected based on similar uranyl compounds.[31] If the reaction is performed with excess ^{dipp}iq ligand, formation of **1-iq** is

still observed, suggesting the triflate anions are not subject to substitution by neutral ^{dipp}iq despite the chelation effect of the bidentate ligand.

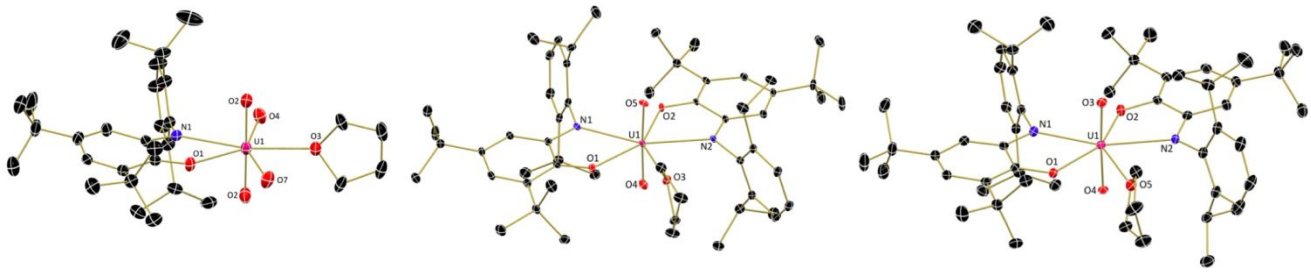

Figure 2. Molecular structure of **1-iq** (left), **2-isq** (middle) and **3-ap crown** (right) shown with 30% probability ellipsoids. Hydrogen atoms, co-crystallized solvent molecules, potassium ions, crown ether molecules and bound triflate ions (except coordinated oxygen atoms) are omitted for clarity.

Table 1: Selected uranyl bond distances (Å) and angles (°) for **1-iq**, **2-isq**, **3-ap**, **3-ap crown** and **4-iq/isq**.

	1-iq	**2-isq**	**3-ap**	**3-ap crown**	**4-iq/isq**
U-O_{Uranyl}	1.745(5)	1.762(4)	1.824(3)	1.812(2)	1.757(3)
U-O_{Uranyl}	1.745(5)	1.786(3)	1.834(3)	1.814(2)	1.758(3)
O_{Uranyl}-U-O_{Uranyl}	179.1(2)	175.42(17)	172.22(12)	174.54(10)	175.09(13)

After successful metalation of the neutral ^{dipp}iq ligand, the redox-active nature of the ligand was engaged by stirring two equivalents of ^{dipp}iq with one equivalent of $UO_2Cl_2(THF)_3$ followed by slow addition of two equivalents of KC_8 (Scheme 1), causing a color change from red/brown to dark green. After workup, a green powder was

isolated in moderate yield (67%). The ^{1}H NMR spectrum (Figure S5) displays broad, paramagnetically-shifted signals ranging from 0 – 55 ppm. In this case, the paramagnetism can arise either from 1) reduction of the uranium (VI) (f^{0}) center to uranium (V) (f^{1}) while maintaining a neutral iminoquinone ligand, or 2) from ligand reduction to generate two radical-containing iminosemiquinone ligands.

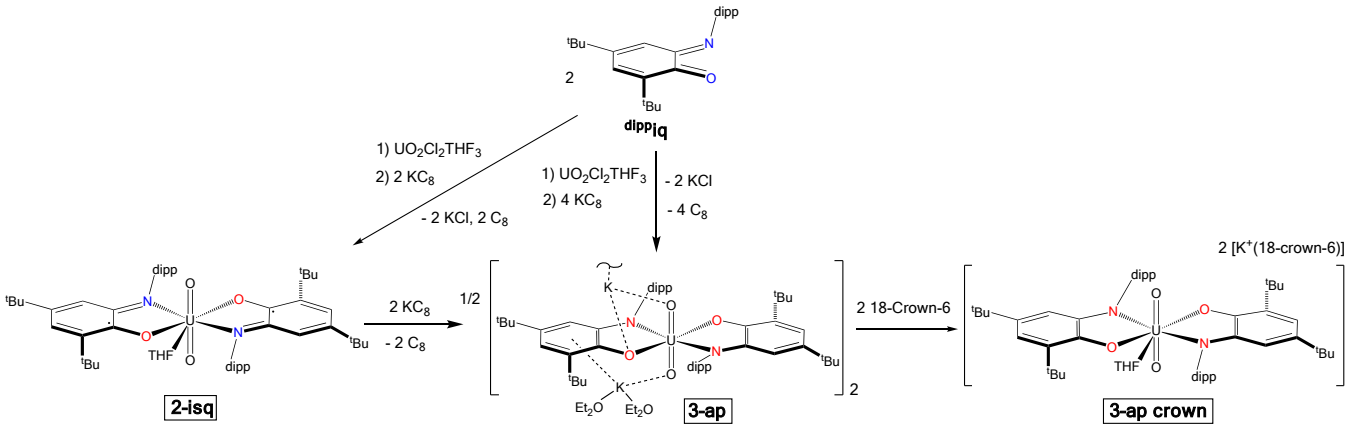

Scheme 1. Synthesis of complexes **2-isq**, **3-ap** and **3-ap crown**.

To further elucidate the electronic structure of **2-isq**,[17, 32, 33] X-ray crystallography was employed as structural parameters, including intraligand bond distances, can often aid in ligand oxidation state assignment.[34] Crystals of **2-isq** grown from diethyl ether at -35 °C were analyzed. Refinement of the data revealed a seven coordinate uranyl species, with two ^{dipp}iq ligands and a THF molecule coordinated in the equatorial plane (Figure 2, middle). As with **1-iq**, a pentagonal bipyramidal geometry with the uranyl oxygen atoms in axial positions was observed. Additionally, the U-O_{uranyl} bond distances of 1.762(4) and 1.786(3) Å (Table 1) are within the range of 1.76 – 1.79 Å

observed for U(VI) uranyl molecules.[31, 32, 35] These U-O_{uranyl} distances suggest the reduction is ligand-based rather than occurring at the uranium.

To further confirm the presence of ligand radicals, EPR spectroscopy was performed. The EPR spectrum of **2-isq** (Figure 3) displays an isotropic signal at g = 1.993, which is shifted from that of 2.0061 observed for 4,6-di-*tert*-butyl-2-*tert*-butyl-iminosemiquinone (H^{tBu}isq•)[36]. This value agrees well with the g-value previously observed for hexavalent uranyl species featuring redox-active ligands, such as $Cp^*UO_2(^{Mes}PDI^{Me})$ (g_{iso} = 1.974), $Cp^*UO_2(^{t}Bu\text{-}^{Mes}PDI^{Me})$ (g_{iso} =1.936) and $[UO_2(salophen)^{tBu}(H_2O)]^+$ (g_{av} =1.997) ($^{t}Bu\text{-}^{Mes}PDI^{Me}$ = 2,6-((Mes)-N=CMe)$_2$-*p*-$C(CH_3)_3C_5H_2N$; salophen = *N*,*N*′-bis(3-^{t}Bu-(5^{t}Bu)-salicylidene)-1,2-phenylenediamine).[17] Spin-orbit coupling of the ligand-based radical with the empty *f*-orbitals of the uranium center is likely the cause of the high-field shift from the g-value observed for H^{tBu}isq•. Simulation of the spectrum was accomplished with one nitrogen (I = 1) and one hydrogen atom (I = ½) of the ligand, yielding hyperfine coupling constants of A_N = 19.48 and A_H = 13.97 MHz. These values suggest a stronger interaction with the nitrogen atom than the hydrogen atom of the ligand. This hyperfine pattern agrees with previously noted results[18, 36]. Thus, these measurements support the presence of an iminosemiquinone ligand radical with only a weak interaction with uranium.

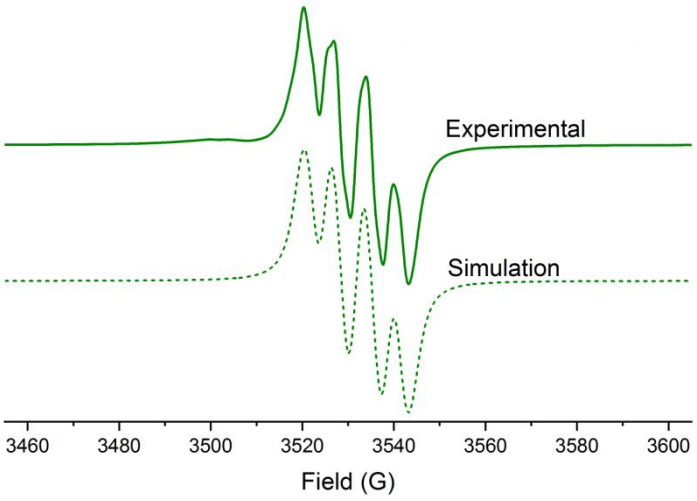

Figure 3. EPR spectrum of **2-isq** (*n*-pentane, 5.8 mM) recorded at 25 °C. g_{iso} = 1.993. Frequency: 9.852 GHz. Power: 10 mW. Modulation: 0.5 G/100 kHz.

Variable-temperature and field-dependent magnetic measurements were performed to elucidate the uranium and ligand oxidation states in **2-isq** (Figure 4). At room temperature, the μ_{eff} value (2.45 μ_B) was consistent with that expected for two isolated, unpaired electrons with g = 2.0 (theoretical μ_{eff} value = 2.45 μ_B).[37] Upon cooling, the μ_{eff} value slightly increased to 2.52 μ_B at 4 K. The increase in moment resulted from the ferromagnetic coupling of the two unpaired electrons. The data were fitted by the Bleaney−Bowers equation[38] with g = 2.00 and exchange coupling constant J = 0.4 cm^{-1} (see the supporting information for details). The magnetization in the field dependent measurement saturated at 1.94 μ_B at 2 K, also characteristic of two isolated S = 1/2 spins.[37] Overall, these magnetic data indicated the presence of one U(VI) cation and two ligand-centered radicals with negligible ferromagnetic coupling in **2-isq**. This value supports the presence of two non-communicating ligand radicals that were measured

by EPR and predicted with the metrical parameters deduced by X-ray crystallography (*vide infra*). The radicals in **2-isq** are relegated to the ligand at all temperatures, with little interaction with the uranium. This rules out alternate potential electronic structures for **2-isq** (Figure 5). These magnetic data also eliminate formation of pentavalent $(isq^{1-})(iq^{0})U^{V}O_2$, which would have both uranium based and ligand based radicals, as well as $(iq^{0})_2U^{IV}O_2$, which would have closed-shell ligands with only uranium based electrons unpaired.

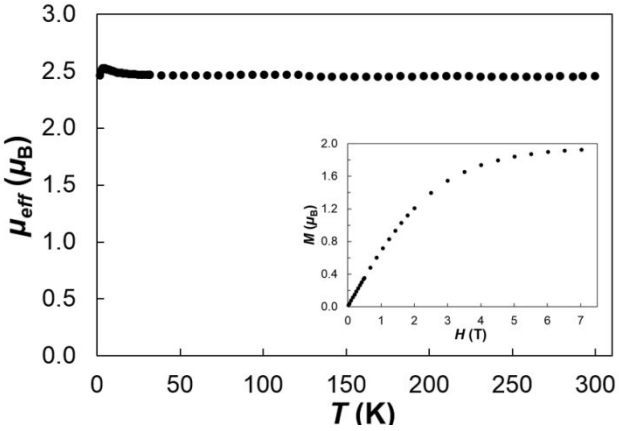

Figure 4. Variable temperature molar magnetic data (μ_{eff}) for **2-isq** and variable field data collected at 2 K (inset)

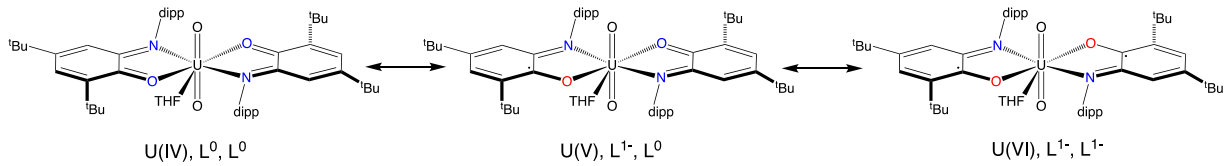

Figure 5. Possible electronic structures of **2-isq**.

To probe the ability of our system to accommodate additional electrons beyond monoreduction of both ligands, electrochemical measurements of **2-isq** were performed

in THF (Figure S19). The cyclic voltammetric data for **2-isq** showed a quasi-reversible reduction at -1.58 V, which could be attributed to the reduction of the two ligands from isq^{1-} to ap^{2-} or reduction of uranium from +6 to +5. Encouraged by the electrochemical results, **2-isq** was reduced chemically by stirring with two equivalents of KC_8 in THF. Following workup, a tan powder that is poorly soluble in hydrocarbon solvents was isolated. ^{1}H NMR spectroscopic analysis (pyridine-d_5) showed a spectrum (Figure S6) with 11 resonances. Of these, nine signals were assigned to the ligand and two signals as bound THF, none of which were drastically shifted from the diamagnetic region. These data suggest a closed-shell U(VI), f^0 ion with ^{dipp}ap ligands bound to uranium.

Because solution behavior can be complicated by dynamic inner-sphere and outer-sphere cation exchange, a crown ether was employed to encapsulate the potassium ion for further studies.[18, 39, 40] To achieve this, two equivalents of 18-crown-6 were added to a stirring solution of **3-ap** in THF. After workup, a white powder was isolated in good yield (76%). The ^{1}H NMR spectrum (Figure S8) is quite similar to that of **3-ap**, with minor differences, including an additional resonance at 3.43 ppm corresponding to the 24 protons associated with 18-crown-6.

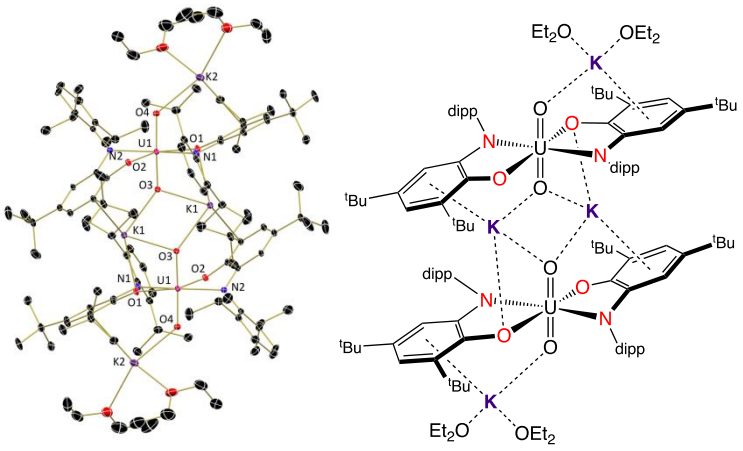

Figure 6. Molecular structure of **3-ap** (left) shown with 30% probability ellipsoids. Co-crystallized solvent molecules and H atoms are omitted for clarity. Schematic representation of **3-ap** (right), with interactions between potassium ions and various parts of the molecule shown as dashed lines.

Comparison of the structural changes that accompany reduction and examination of the effect of potassium ion sequestration in **3-ap** (Figure 6) and **3-ap crown** (Figure 2, right) were examined using X-ray crystallography. **3-ap** crystallizes as a dimer from diethyl ether or toluene at -35 °C with the oxygen atom and aromatic ring of the ^{dipp}iq ligand, and uranyl oxygen atoms interacting with the potassium ions. This dimerization causes out of plane bending of the ligand with the N and O atoms appearing to be sp^3 hybridized to allow for lone pair interaction with the nearby potassium ions. Additionally, the uranyl bond distances of 1.824(3) and 1.834(3) Å (Table 1) are quite long,[31] appearing to result from the potassium binding to the O_{uranyl}. This cation-capping effect has been thoroughly studied by P. Arnold and coworkers who employed a large, compartmental, N_8-macrocyclic ligand.[41] In these studies,

reduction of uranyl was facilitated by coordination of a cation, held in place by the specialized "Pacman" type ligand, to the O_{uranyl}.

The structure of **3-ap crown** shows that sequestering the potassium ions with crown ethers permits the amidophenolate ligands to return to their planar geometry, isostructural to **2-isq**. Interestingly, despite the absence of the interaction of potassium atoms with the uranyl moiety in **3-ap crown**, the U-O_{uranyl} bond distances remain long (1.814(2) and 1.812(2) Å), suggesting ligand reduction plays a role in the elongation of the U-O_{uranyl} bond. This implies that cation coordination is not the only contributing factor in the U-O_{uranyl} bond elongation observed in **3-ap**. U-O_{uranyl} bond lengthening has been previously observed by Hayton and co-workers when they described tris- and tetrakis-ketimide complexes $[Li(THF)(TMEDA)][UO_2(N=C^tBuPh)_3]$ and $[Li(THF)(Et_2O)]_2[UO_2(N=C^tBuPh)_4]$.[42] These ketimide uranyl molecules display U-O_{uranyl} bond lengths of 1.830(5) and 1.804(5) Å (tris-ketimide) and 1.838(4) Å (tetrakis-ketimide). The authors attribute this elongation to the presence of four strong donors in the equatorial plane, which act to weaken the U-O_{uranyl} bonds via electrostatic repulsion and π-donation to the uranium center. Further evidence of this elongation can be found in the imido family of uranyl analogues. Studies of uranium tris-[43] and tetrakis(imidos)[44] – featuring strong π-donating imido groups in the equatorial plane – have shown that imido bonds lengthen and weaken with each additional π-donor. The $^{dipp}ap^{2-}$ ligand has been studied as a π-donating ligand for high valent metals previously.[24] As its high-lying π orbitals have the appropriate symmetry to donate electron density to the

uranium VI center, this is likely a factor in U-O_{uranyl} bond elongation and activation in **3-ap crown**.

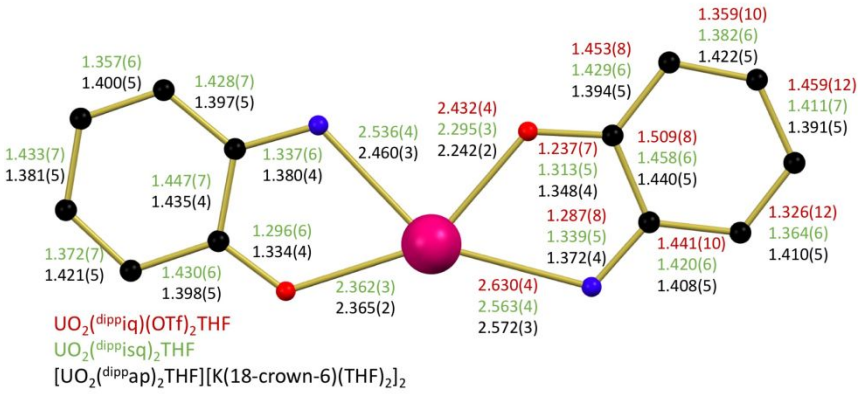

Figure 7. Bond distance comparison (Å) for **1-iq**, **2-isq**, and **3-ap crown**. Carbon atoms shown in black, nitrogen atoms shown in blue, oxygen atoms shown in red, and uranium atom shown in magenta.

The bond metrics vary based on the ligand oxidation state, and can therefore provide insight into the electronic structure of **1-iq**, **2-isq**, and **3-ap crown** (Figure 7). The neutral ^{dipp}iq ligand of **1-iq** displays relatively long uranium-oxygen (2.432(4) Å) and uranium-nitrogen (2.630(4) Å) bonds that are indicative of a datively bound ligand. Furthermore, the short C-O (1.237(7) Å) and C-N (1.287(8) Å) bonds suggest the ligand retains double bond character. In contrast, the iminosemiquinone ligands of **2-isq** feature shortened U-O bonds (2.295(3) and 2.362(3) Å) and U-N bonds (2.563(4) and 2.536(4)) accompanied by longer C-O (1.313(5) and 1.296(6) Å) and C-N bonds (1.339(5) and 1.337(6) Å), indicating reduction of the ligand.

The bond distances of **3-ap crown** are not as simple to analyze as those of the other compounds of the series. While the expected shortening trend of the U-E (E = O, N) bond is observed for one "E" atom of each ligand, the other "E" atom bond distance is nearly identical to that of **2-isq**. This could be attributed to steric hindrance with the bulky dipp or ^{t}Bu groups that prevent the U-E bonds from contracting towards the metal center upon reduction. In this case, a stronger indication of reduction can be found in the intraligand bond distances (Figure 7). The C-O and C-N bonds in each ligand lengthen, signifying the conversion from a double bond to a single bond. Corroborating evidence can also be found in the C-C bond distances of the rings in the ligands. As the ligand is reduced, the distances throughout the ring become more similar, suggesting aromaticity is present.

As the bond distances in molecules **1-iq**, **2-isq** and **3-ap crown** change with ligand oxidation state, the bond angles also indicate ligand reduction. In particular, this effect is noticeable in the N_{iq}-U-O_{iq} angles of the iminoquinone ligand. As the ligand becomes more reduced, the shortening of the U-O_{iq} and U-N_{iq} bonds causes the N_{iq}-U-O_{iq} bite angle of the ligand to increase from 61.83° (**1-iq**) to 64.44° (**2-isq**) and finally to 65.26° (**3-ap crown**).

Another useful technique for examining the ligand and metal oxidation states in uranium/uranyl systems is electronic absorption spectroscopy. For the current study, this technique is particularly advantageous as **1-iq**, **2-isq**, and **3-ap** all exhibit distinctly different colors (Figure S16 and S17). Spectra were recorded in THF at 25 °C from 375 –

1800 nm. The spectrum of **1-iq** displays an intense absorption at 385 nm (41,711 $M^{-1}cm^{-1}$) with a weaker absorption at 511 nm (4,075 $M^{-1}cm^{-1}$), giving rise to the observed red-purple color. **2-isq** shows an intense absorption at 310 nm (26,600 $M^{-1}cm^{-1}$) and a much less intense, broad absorption at 747 nm (2,130 $M^{-1}cm^{-1}$), responsible for the observed green color. Finally, **3-ap** shows only one absorption at 313 nm (15,313 $M^{-1}cm^{-1}$) and does not absorb significantly in the visible region, consistent with its pale color. Interpretation of these data suggests that the major, color-producing peaks of the spectra can be attributed to the ligand oxidation state, as similar colors have been observed for complexes of early transition metals[20], lanthanides[18], and low valent uranium.[21]

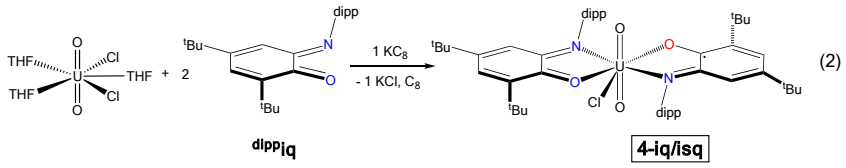

(2)

Synthesis and Characterization of a Mixed Ligand Species. The extent of radical delocalization in the uranyl iminoquinone complexes was tested by synthesizing a mixed iminoquinone/iminosemiquinone ligand species. We hypothesized that rather than full delocalization of the radical across both ligands, the radical would remain localized on one of the iminosemiquinone ligands and not the other. Preparation of (^{dipp}iq)(^{dipp}isq)UO_2Cl **(4-iq/isq)** was achieved by stirring two equivalents of the iminoquinone ligand with one equivalent of uranyl chloride in the presence of one

equivalent of potassium graphite (Eq. 2). Upon workup, a greenish-brown powder was isolated in moderate yield (66%).

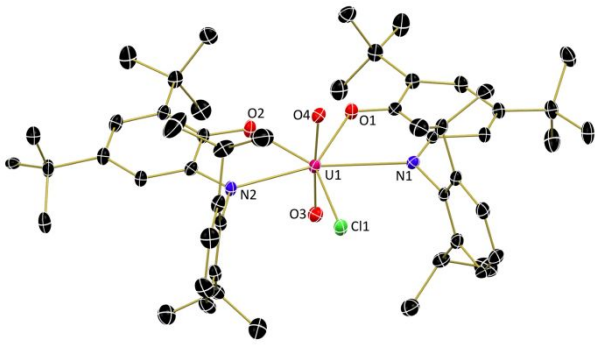

Figure 8. Molecular structure of **4-iq/isq** shown with 30% probability ellipsoids. Co-crystallized solvent molecules and H atoms are omitted for clarity.

X-ray crystallographic analysis of green-brown crystals grown from diethyl ether show a pentagonal bipyramidal uranium center similar to that of **2-isq** but with a chloride atom instead of a THF molecule (Figure 8, Table 1). Compound **4-iq/isq** shows asymmetric ligands in the solid state, with each ligand's oxidation state undoubtedly assignable based on bond distances (Figure 9). The U-O distances of 2.493(3) and 2.312(3) Å and U-N distances of 2.670(3) and 2.498(3) Å highlight the asymmetric nature of the two ligands, with the shorter contact belonging to the isq ligand and the longer to the iq ligand. Further evidence can be found in the C-O and C-N distances, as well as the intraligand C-C distances. For the iminoquinone ligand, C-O and C-N bonds of 1.230(5) and 1.290(5) Å are indicative of double bond character, as observed for **1-iq**. However, the C-O and C-N bonds of the other ligand are significantly longer at 1.297(5) and 1.341(5) Å, agreeing well with the ligands of **2-isq**. Additional evidence can be found in the C-C bonds of each ring, with the iminoquinone ligand featuring two short bonds and three long ones,

whereas the iminosemiquinone ligand has bonds more similar in length. Both of these trends match well with the ligands of compounds **1-iq** and **2-isq**, respectively.

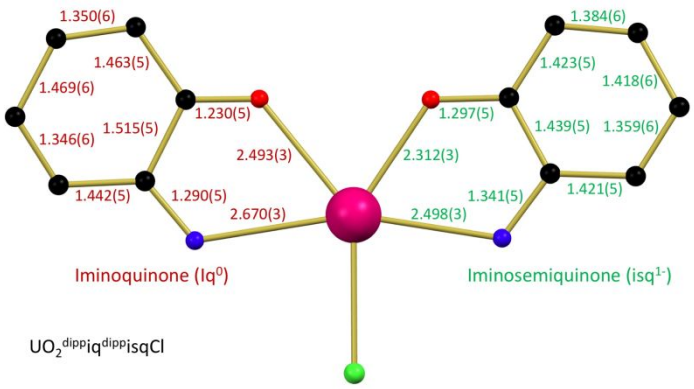

Figure 9. Bond distance comparison (Å) for **4-iq/isq**. Carbon atoms shown in black, nitrogen atoms shown in blue, oxygen atoms shown in red, chloride atoms shown in green and uranium atom shown in magenta.

The presence of a ligand radical in **4-iq/isq** was confirmed using EPR spectroscopy (Figure S18). In a toluene solution, an isotropic signal is observed at g = 1.989. This is comparable to the g-value of **2-isq** (1.993). Variable temperature SQUID magnetometry provides additional evidence of the ligand radical (Figure S25), which establishes a room temperature μ_{eff} value of 1.86 μ_B. The UV-Vis/NIR spectrum of **4-iq/isq** displays absorbance in multiple regions (Figure S16 and S17), which explains the observed brown color. Intense absorbances are noted at 307 nm (15,188 $M^{-1}cm^{-1}$) and 388 nm (5759 $M^{-1}cm^{-1}$), while signals at 528 nm (259 $M^{-1}cm^{-1}$) and 800 nm (839 $M^{-1}cm^{-1}$) are broad and less intense. The number of absorbance maxima is likely the product of the ligands existing in two oxidation states, absorbing at different wavelengths.

Uranyl Functionalization

Reactivity of 2-isq with B-Chlorocatecholborane. Boron is well-known for its Lewis acidic properties, making it an excellent candidate to examine reactivity with electron-rich **2-isq**. B-chlorocatecholborane (Cl-BCat) features a B-Cl bond that can be heterolytically cleaved by the chlorophilic uranium. Treating **2-isq** with four equivalents of Cl-BCat causes the solution to change color from green to brown immediately. Resonances in the ^{1}H NMR spectrum of the reaction mixture (Figure S11) range from -20 to +20 ppm, suggesting that the uranyl was reduced to paramagnetic U(IV), f^2, a transformation that likely involves uranyl U-O_{uranyl} bond activation (Eq. 3). Further inspection of the data, coupled with ^{11}B NMR data (Figure S12), revealed that dicatecholatobisborylether ($BOBCat_2$) was produced during the reaction. In sealed-tube NMR experiments in benzene-d_6 and THF-d_8, free ligand is also observed, but does not integrate to one full equivalent. Based on the stoichiometry of Cl-BCat and the number and integration values of resonances in the ^{1}H NMR spectrum, the resulting uranium product was hypothesized to be $UCl_4(^{dipp}iq^0)_n$ (n = 1, 2).

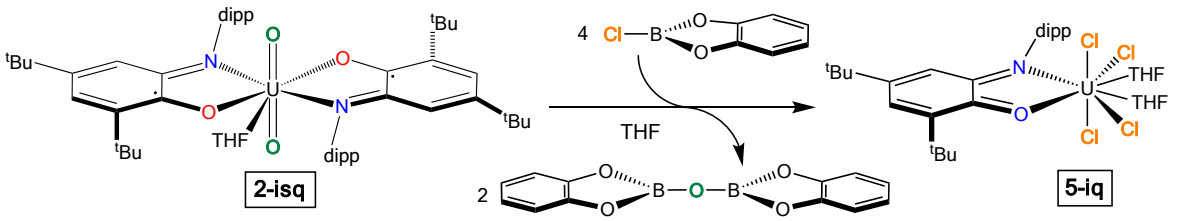

(3)

Identification of the U(IV) product from borylation of **2-isq** was achieved by an independent synthesis. Treating UCl_4 with an equivalent of ^{dipp}iq in THF produced a

dark green solution (Eq. 4), and ^{1}H NMR data confirmed the product was the same as that observed in the uranyl borylation reaction (Figure S14). The material from the independent synthesis was crystallized from THF and subsequent X-ray analysis revealed the identity to be $UCl_4{}^{dipp}iq(THF)_2$ (**5-iq**) (Figure S23). The ligands are confirmed to be in the iminoquinone form with C-O and C-N distances of 1.234(3) and 1.298(3) Å, signifying double bonds and matching the distances observed in **1-iq** and **4-iq/isq**. Further evidence can be found in the U-O and U-N distances of 2.4878(16) and 2.8283(18) Å, which are longer than the contacts reported for iminosemiquinone-containing U(IV) complexes $(^{tBu}isq)_2UI_2(THF)$ (U-O = 2.160(10) and 2.164(10), U-N = 2.514(12) and 2.567(14) Å).[21] These longer contacts highlight the dative nature of the ligand binding in **5-iq**.

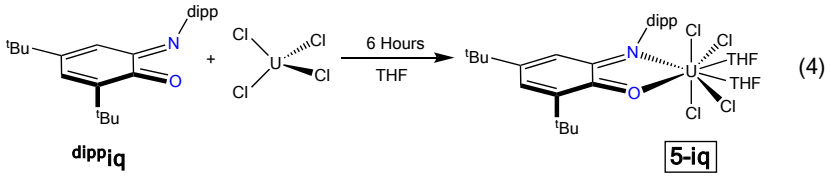

(4)

To corroborate that the organic products observed were the result of U-O_{uranyl} bond cleavage and that the extracted oxygen atoms had originated from the U-O_{uranyl}, isotopic labeling studies were performed. ^{18}O-labeled uranyl dichloride ($[U^{18}O_2Cl_2(THF)_2]_2$) was synthesized through photolysis of uranyl chloride hydrate in ^{18}O-labeled water.[31] ^{18}O incorporation was confirmed by IR spectroscopy, with the expected OUO asymmetric stretching frequency reducing from 942.4 cm^{-1} ($[U^{16}O_2Cl_2(THF)_2]_2$) to 892.3 cm^{-1} ($[U^{18}O_2Cl_2(THF)_2]_2$) (Figure S20). Synthesis of

(^{dipp}isq)$_2$U^{18}O$_2$THF (**2-isq^{18}**) was accomplished in an analogous manner to **2-isq**, using [U^{18}O$_2$Cl$_2$(THF)$_2$]$_2$ as the uranyl source. Successful incorporation was confirmed by IR spectroscopy (Figure S21).

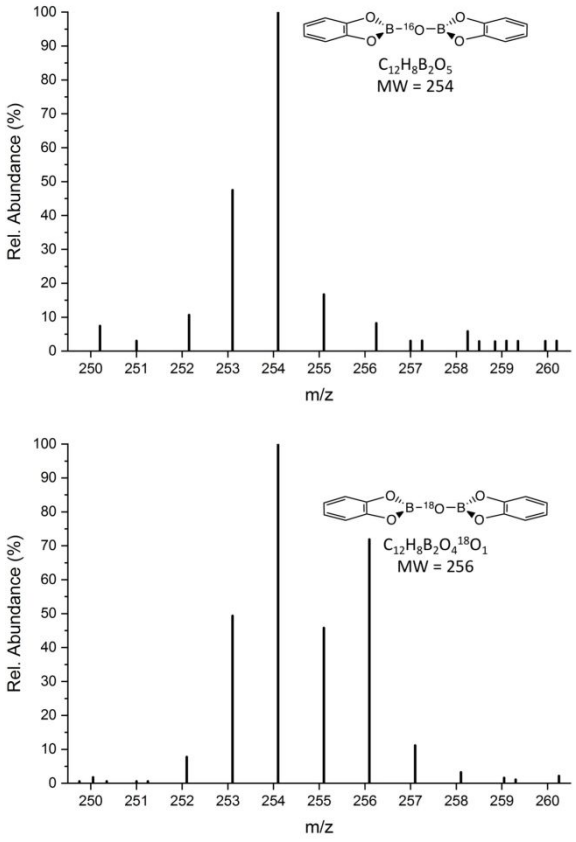

Figure 10. Electron ionization mass spectra (EI-MS) of BOBCat$_2$ from the reaction mixture of ClBCat and **2-isq** (top) and **2-isq^{18}** (bottom).

Treating **2-isq^{18}** with Cl-BCat under the same conditions as previously described for the unlabeled isotopomer yielded analogous results as identified by ^{1}H and ^{11}B NMR spectroscopies. Analysis of the organic bisborylether, B^{18}OBCat$_2$, by EI-MS gave an increase in the M$^{\bullet+}$ peak appearing at m/z = 256, corresponding to the incorporation

of one ^{18}O-labeled oxygen atom. $BOBCat_2$, obtained from the borylation of **2-isq**, shows an analogous peak at m/z = 254 (Figure 10, top). The shift from m/z of 254 to 256 is indicative of ^{18}O incorporation and supports that the source of the oxygen atom in $BOBCat_2$ is from the labeled uranyl $U\text{-}O_{uranyl}$.

Reactivity of 2-isq with Pivaloyl Chloride. Upon establishing that **2-isq** could mediate $U\text{-}O_{uranyl}$ bond cleavage with Cl-BCat, we hypothesized that an analogous electrophilic carbon could be used to activate the uranyl ion. Pivaloyl chloride (Piv-Cl) was an attractive choice, as the *tert*-butyl group provides steric pressure to aid product dissociation. Treating **2-isq** with four equivalents of pivaloyl chloride in benzene results in no observable reaction. Heating this solution to 50 °C for four hours causes a color change from green to brown. Analysis of the reaction mixture by ^1H NMR revealed a singlet at 1.04 ppm and disappearance of the resonance at 0.89 ppm, suggesting conversion of pivaloyl chloride to pivalic anhydride. Additionally, resonances ranging from -80 to +60 ppm (Figure S13) show that a paramagnetic product is formed; however, these resonances do not match that of **5-iq**. We hypothesized that in the non-coordinating benzene solution, ligand displacement would not occur as in the borylation, which was performed in THF. To confirm this, UCl_4 was treated with two equivalents of iminoquinone in benzene and heating to 50 °C for 18 hours yields an NMR spectrum matching that of the acylation reaction, with no free ligand observed. In the absence of THF, a bis-ligand U(IV) complex, $UCl_4(^{dipp}iq^0)_2$ (**6-iq**), is formed (Figure S15). These spectroscopic results suggest that the two pivaloyl chloride molecules were

able to exchange their chloride atoms for the oxygen atom of a uranyl ion, producing pivalic anhydride (Eq. 5), which is then displaced from the uranium ion.

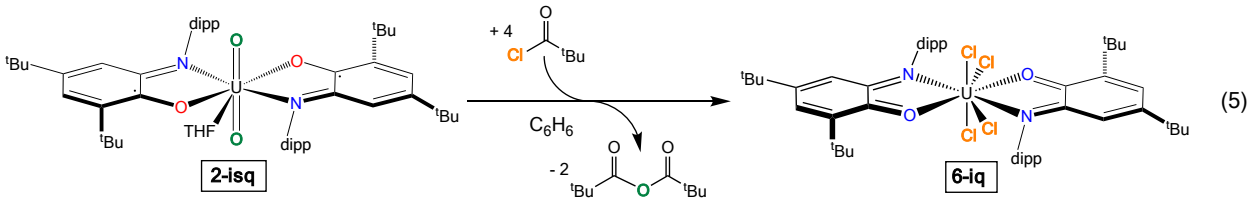

(5)

Reactions of **2-isq** and **2-isq**[18] were performed with pivaloyl chloride, and the organic anhydrides isolated and examined using CI-MS. The labile nature of the C-O bonds in pivalic anhydride causes dissociation in the mass spectrometer, thus, only the protonated carboxylic acid was detected (Figure S22). In the case of the unlabeled sample, a $[M+H]^+$ peak at m/z = 103 was observed. The data for the ^{18}O-labeled sample display an additional $[M+H]^+$ peak m/z = 105, assignable as the ^{18}O-labeled isotopomer. Based on the ratio of these peaks in the labeled sample, the percent incorporation of ^{18}O was calculated to be about 35%. These results, along with the spectroscopic data (*vide supra*), support that U-O_{uranyl} bonds are broken in the process of borylation and acylation, and the oxygen atoms in the organic byproducts originate from the U-O_{uranyl} bond.

Conclusion

In summary, a family of uranyl complexes bearing redox-active ligands has been isolated in three different oxidation states. Thorough characterization has provided insight into their electronic structures. Upon reduction, electrons are stored in the

ligand π* orbitals rather than in uranium based orbitals, retaining the U(VI) oxidation state throughout the series. Notably, **2-isq** has two isolated, ligand-based radicals that can be harnessed for U-O_{uranyl} bond activation. U-O_{uranyl} bond functionalization and scission was carried out with B-chlorocatecholborane or pivaloyl chloride, furnishing either mono- or bis-iminoquinone U(IV) products and the corresponding organic ethers. The origin of the oxygen atom was established by isotopic labeling experiments. Formation of a C-O bond followed by complete U-O cleavage from a uranyl species is unprecedented, with previous examples limited to typical Lewis acidic atoms.

The expansion and understanding of ligand bonding and electronic structure in uranyl compounds is a crucial part of the processing and remediation of uranium in the environment. We have examined this bonding thoroughly with a variety of analytical techniques and exploited the activation of U-O_{uranyl} bonds to convert U(VI) to U(IV) with electrons stored in the iminoquinone ligand. The ability to convert U(VI) to U(IV) is an important requirement in manipulating uranium in the environment and would be a fundamental step in any catalytic cycle featuring high valent uranium. Future experiments will aim to generalize the coordination environment and expand the family of reagents capable of U-O_{uranyl} bond functionalization.

ASSOCIATED CONTENT

Supporting Information. The following files are available free of charge via the Internet at http://pubs.acs.org.

Crystallographic details (CIF)

Additional experimental procedures, spectroscopic data, and crystallographic details (PDF)

AUTHOR INFORMATION

Corresponding Author

*Email: sbart@purdue.edu

ORCID

Ezra J. Coughlin 0000-0002-9938-6649

Yusen Qiao 0000-0001-7654-8636

Eric J. Schelter 0000-0002-8143-6206

Matthias Zeller 0000-0002-3305-852X

Suzanne C. Bart 0000-0002-8918-9051

Notes

The authors declare no competing financial interest.

Acknowledgements

This material is based upon work supported by the U.S. Department of Energy, Office of Science, Office of Basic Energy Sciences under Award Number DE-SC0008479. E. J. S. acknowledges the U.S. Department of Energy, Office of Science, Office of Basic Energy Sciences, Separation Science program under Award Number DE-SC0017259 for financial support. The X-ray crystallographic data in this work was obtained on instruments funded by the National Science Foundation through the Major Research Instrumentation Program under Grant No. CHE 1625543. The authors acknowledge

Professor Jay Kikkawa (Dept. of Physics, University of Pennsylvania) for assistance with the magnetic measurements.

References

1. Greenwood, N. N.; Earnshaw, A., *Chemistry of the Elements*. 2nd ed.; Butterworth Heinemann: Oxford, 1998.
2. Briner, W. E. "The Evolution of Depleted Uranium as an Environmental Risk Factor: Lessons from Other Metals" *Int. J. Environ. Res. Public Health* **2006,** 3, 129-135.
3. Amme, M.; Wiss, T.; Thiele, H.; Boulet, P.; Lang, H. "Uranium Secondary Phase Formation During Anoxic Hydrothermal Leaching Processes of UO_2 Nuclear Fuel" *J. Nucl. Mater.* **2005,** 341, 209-223.
4. DeLemos, J. L.; Bostick, B. C.; Quicksall, A. N.; Landis, J. D.; George, C. C.; Slagowski, N. L.; Rock, T.; Brugge, D.; Lewis, J.; Durant, J. L. "Rapid Dissolution of Soluble Uranyl Phases in Arid, Mine-Impacted Catchments near Church Rock, Nm" *Environ. Sci. Technol.* **2008,** 42, 3951-3957.
5. Arnold, P. L.; Love, J. B.; Patel, D. "Pentavalent Uranyl Complexes" *Coord. Chem. Rev.* **2009,** 253, 1973-1978.
6. Kannan, S.; Moody, M. A.; Barnes, C. L.; Duval, P. B. "Fluoride Abstraction and Reversible Photochemical Reduction of Cationic Uranyl(VI) Phosphine Oxide Complexes" *Inorg. Chem.* **2006,** 45, 9206-9212.
7. Kiernicki, J. J.; Zeller, M.; Bart, S. C. "Facile Reductive Silylation of UO_2^{2+} to Uranium(IV) Chloride" *Angew. Chem. Int. Ed.* **2017,** 56, 1097-1100.
8. Arnold, P. L.; Jones, G. M.; Odoh, S. O.; Schreckenbach, G.; Magnani, N.; Love, J. B. "Strongly Coupled Binuclear Uranium-Oxo Complexes from Uranyl Oxo Rearrangement and Reductive Silylation" *Nat Chem* **2012,** 4, 221-227.
9. Arnold, P. L.; Pecharman, A.-F.; Lord, R. M.; Jones, G. M.; Hollis, E.; Nichol, G. S.; Maron, L.; Fang, J.; Davin, T.; Love, J. B. "Control of Oxo-Group Functionalization and Reduction of the Uranyl Ion" *Inorg Chem* **2015,** 54, 3702-3710.
10. Brown, J. L.; Mokhtarzadeh, C. C.; Lever, J. M.; Wu, G.; Hayton, T. W. "Facile Reduction of a Uranyl(VI) Beta-Ketoiminate Complex to U(IV) Upon Oxo Silylation" *Inorg. Chem.* **2011,** 50, 5105-5112.
11. Kiernicki, J. J.; Harwood, J. S.; Fanwick, P. E.; Bart, S. C. "Reductive Silylation of $Cp^*UO_2(^{Mes}PDI^{Me})$ Promoted by Lewis Bases" *Dalton Trans.* **2016,** 45, 3111-3119.
12. Pedrick, E. A.; Wu, G.; Hayton, T. W. "Reductive Silylation of the Uranyl Ion with Ph_3SiOTf" *Inorg. Chem.* **2014,** 53, 12237-12239.
13. Pedrick, E. A.; Wu, G.; Kaltsoyannis, N.; Hayton, T. W. "Reductive Silylation of a Uranyl Dibenzoylmethanate Complex: An Example of Controlled Uranyl Oxo Ligand Cleavage" *Chem. Sci.* **2014,** 5, 3204-3213.
14. Jones, G. M.; Arnold, P. L.; Love, J. B. "Oxo–Group-14-Element Bond Formation in Binuclear Uranium(V) Pacman Complexes" *Chem. – Eur. J.* **2013,** 19, 10287-10294.

15. Arnold, P. L.; Mansell, S. M.; Maron, L.; McKay, D. "Spontaneous Reduction and C-H Borylation of Arenes Mediated by Uranium(III) Disproportionation" *Nature Chem* **2012,** 4, 668-674.
16. Cowie, B. E.; Nichol, G. S.; Love, J. B.; Arnold, P. L. "Double Uranium Oxo Cations Derived from Uranyl by Borane or Silane Reduction" *Chemical Communications* **2018,** 54, 3839-3842.
17. Kiernicki, J. J.; Cladis, D. P.; Fanwick, P. E.; Zeller, M.; Bart, S. C. "Synthesis, Characterization, and Stoichiometric U=O Bond Scission in Uranyl Species Supported by Pyridine(Diimine) Ligand Radicals" *J. Am. Chem. Soc.* **2015,** 137, 11115-11125.
18. Coughlin Ezra, J.; Zeller, M.; Bart Suzanne, C. "Neodymium(III) Complexes Capable of Multi-Electron Redox Chemistry" *Angew. Chem.* **2017,** 129, 12310-12313.
19. Blackmore, K. J.; Ziller, J. W.; Heyduk, A. F. ""Oxidative Addition" to a Zirconium(IV) Redox-Active Ligand Complex" *Inorg. Chem.* **2005,** 44, 5559-5561.
20. Blackmore, K. J.; Sly, M. B.; Haneline, M. R.; Ziller, J. W.; Heyduk, A. F. "Group IV Imino-Semiquinone Complexes Obtained by Oxidative Addition of Halogens" *Inorg. Chem.* **2008,** 47, 10522-10532.
21. Matson, E. M.; Opperwall, S. R.; Fanwick, P. E.; Bart, S. C. ""Oxidative Addition" of Halogens to Uranium(IV) Bis(Amidophenolate) Complexes" *Inorg. Chem.* **2013,** 52, 7295-7304.
22. Matson, E. M.; Franke, S. M.; Anderson, N. H.; Cook, T. D.; Fanwick, P. E.; Bart, S. C. "Radical Reductive Elimination from Tetrabenzyluranium Mediated by an Iminoquinone Ligand" *Organometallics* **2014,** 33, 1964-1971.
23. Abakumov, G. A.; Cherkasov, V. K.; Piskunov, A. V.; Meshcheryakova, I. N.; Maleeva, A. V.; Poddel'skii, A. I.; Fukin, G. K. "Zinc Molecular Complexes with Sterically Hindered O-Quinone and O-Iminoquinone" *Dokl. Chem.* **2009,** 427, 168-171.
24. Ranis, L. G.; Werellapatha, K.; Pietrini, N. J.; Bunker, B. A.; Brown, S. N. "Metal and Ligand Effects on Bonding in Group 6 Complexes of Redox-Active Amidodiphenoxides" *Inorg. Chem.* **2014,** 53, 10203-10216.
25. Pangborn, A. B.; Giardello, M. A.; Grubbs, R. H.; Rosen, R. K.; Timmers, F. J. "Safe and Convenient Procedure for Solvent Purification" *Organometallics* **1996,** 15, 1518-1520.
26. Chakraborty, S.; Chattopadhyay, J.; Guo, W.; Billups, W. E. *Angew. Chem. Int. Ed.* **2007,** 46, 4486-4488.
27. Wilkerson, M. P.; Burns, C. J.; Paine, R. T.; Blosch, L. L.; Andersen, R. A. "Organometallic and Coordination Complexes. Di(M-Chloro)Bis{Chlorodioxobis(Tetrahydrofuran)Uranium(VI)}, $[UO_2Cl_2(THF)_2]_2$" *Inorg. Synth.* **2004,** 34, 93-95.
28. Berthet, J. C.; Lance, M.; Nierlich, M.; Ephritikhine, M. "Simple Preparations of the Anhydrous and Solvent-Free Uranyl and Cerium(IV) Triflates $UO_2(OTf)_2$ and $Ce(OTf)_4$ - Crystal Structures of $UO_2(OTf)_2(Py)_3$ and $[\{UO_2(Py)_4\}_2(\mu\text{-}O)][OTf]_2$" *Eur. J. Inorg. Chem.* **2000**, 1969-1973.
29. Kiplinger, J. L.; Morris, D. E.; Scott, B. L.; Burns, C. J. "Convenient Synthesis, Structure, and Reactivity of $(C_5Me_5)U(CH_2C_6H_5)_3$: A Simple Strategy for the Preparation

of Monopentamethylcyclopentadienyl Uranium(Iv) Complexes" *Organometallics* **2002,** 21, 5978-5982.
30. Abergel, R. J.; de Jong, W. A.; Deblonde, G. J. P.; Dau, P. D.; Captain, I.; Eaton, T. M.; Jian, J.; van Stipdonk, M. J.; Martens, J.; Berden, G.; Oomens, J.; Gibson, J. K. "Cleaving Off Uranyl Oxygens through Chelation: A Mechanistic Study in the Gas Phase" *Inorg. Chem.* **2017,** 56, 12930-12937.
31. Fortier, S.; Hayton, T. W. "Oxo Ligand Functionalization in the Uranyl Ion (UO_2^{2+})" *Coord. Chem. Rev.* **2010,** 254, 197-214.
32. Herasymchuk, K.; Chiang, L.; Hayes, C. E.; Brown, M. L.; Ovens, J.; Patrick, B. O.; Leznoff, D. B.; Storr, T. "Synthesis and Electronic Structure Determination of Uranium(VI) Ligand Radical Complexes" *Dalton Trans.* **2016,** 45, 12576-12586
33. Takao, K.; Tsushima, S.; Ogura, T.; Tsubomura, T.; Ikeda, Y. "Experimental and Theoretical Approaches to Redox Innocence of Ligands in Uranyl Complexes: What Is Formal Oxidation State of Uranium in Reductant of Uranyl(VI)?" *Inorg. Chem.* **2014,** 53, 5772-5780.
34. Budzelaar, P. H. M.; de Bruin, B.; Gal, A. W.; Wieghardt, K.; van Lenthe, J. H. "Metal-to-Ligand Electron Transfer in Diiminopyridine Complexes of Mn-Zn. A Theoretical Study" *Inorg. Chem.* **2001,** 40, 4649-4655.
35. Azam, M.; Al-Resayes, S. I.; Velmurugan, G.; Venuvanalingam, P.; Wagler, J.; Kroke, E. "Novel Uranyl(VI) Complexes Incorporating Propylene-Bridged Salen-Type N_2O_2-Ligands: A Structural and Computational Approach" *Dalton Trans.* **2015,** 44, 568-577.
36. Carter, S. M.; Sia, A.; Shaw, M. J.; Heyduk, A. F. "Isolation and Characterization of a Neutral Imino-Semiquinone Radical" *J. Am. Chem. Soc.* **2008,** 130, 5838-5839.
37. Kahn, O., *Molecular Magnetism*. Wiley-VCH: New York, NY, 1993; p 396.
38. Bleaney, B.; Bowers, K. D. "Anomalous Paramagnetism of Copper Acetate" *Proc. R. Soc. London, Ser. A: Mathematical and Physical Sciences* **1952,** 214, 451.
39. Cobb, P. J.; Moulding, D. J.; Ortu, F.; Randall, S.; Wooles, A. J.; Natrajan, L. S.; Liddle, S. T. "Uranyl-Tri-Bis(Silyl)Amide Alkali Metal Contact and Separated Ion Pair Complexes" *Inorg. Chem.* **2018,** 57, 6571-6583.
40. Arnold, P. L.; Stevens, C. J.; Bell, N. L.; Lord, R. M.; Goldberg, J. M.; Nichol, G. S.; Love, J. B. "Multi-Electron Reduction of Sulfur and Carbon Disulfide Using Binuclear Uranium(III) Borohydride Complexes" *Chem. Sci.* **2017,** 8, 3609-3617.
41. Arnold, P. L.; Patel, D.; Wilson, C.; Love, J. B. "Reduction and Selective Oxo Group Silylation of the Uranyl Dication" *Nature* **2008,** 451, 315-317.
42. Seaman, L. A.; Pedrick, E. A.; Wu, G.; Hayton, T. W. "Promoting Oxo Functionalization in the Uranyl Ion by Ligation to Ketimides" *J. Organomet. Chem.* **2018,** 857, 34-37.
43. Anderson, N. H.; Odoh, S. O.; Yao, Y.; Williams, U. J.; Schaefer, B. A.; Kiernicki, J. J.; Lewis, A. J.; Goshert, M. D.; Fanwick, P. E.; Schelter, E. J.; Walensky, J. R.; Gagliardi, L.; Bart, S. C. "Harnessing Redox Activity for the Formation of Uranium Tris(Imido) Compounds" *Nat. Chem.* **2014,** 6, 919-926.

44. Anderson, N. H.; Xie, J.; Ray, D.; Zeller, M.; Gagliardi, L.; Bart, S. C. "Elucidating Bonding Preferences in Tetrakis(Imido)Uranate(VI) Dianions" *Nat. Chem.* **2017,** 9, 850-855.

TOC Graphic:

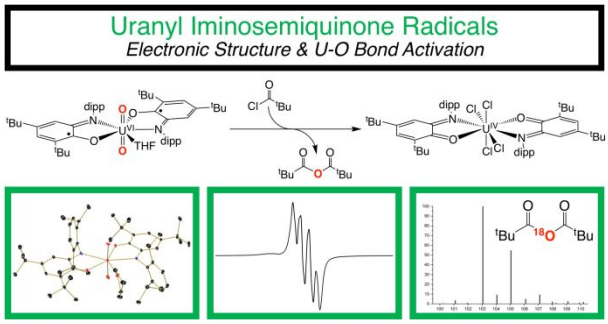

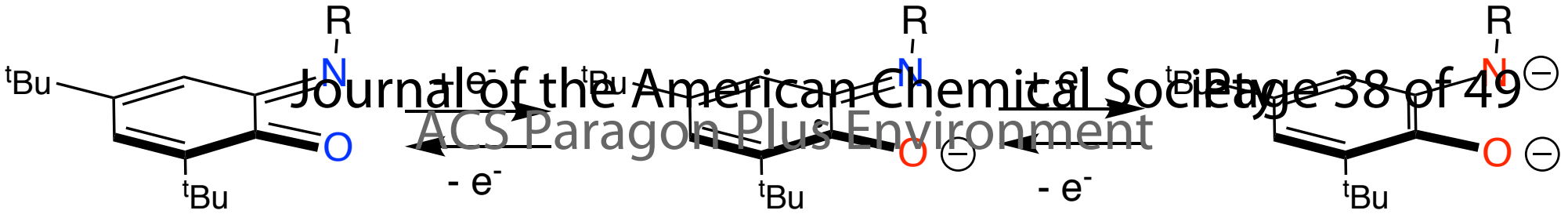

Iminoquinone
iq^0

Iminosemiquinone
isq^{1-}

Amidophenolate
ap^{2-}

1

(1)

^{dipp}iq **1-iq**

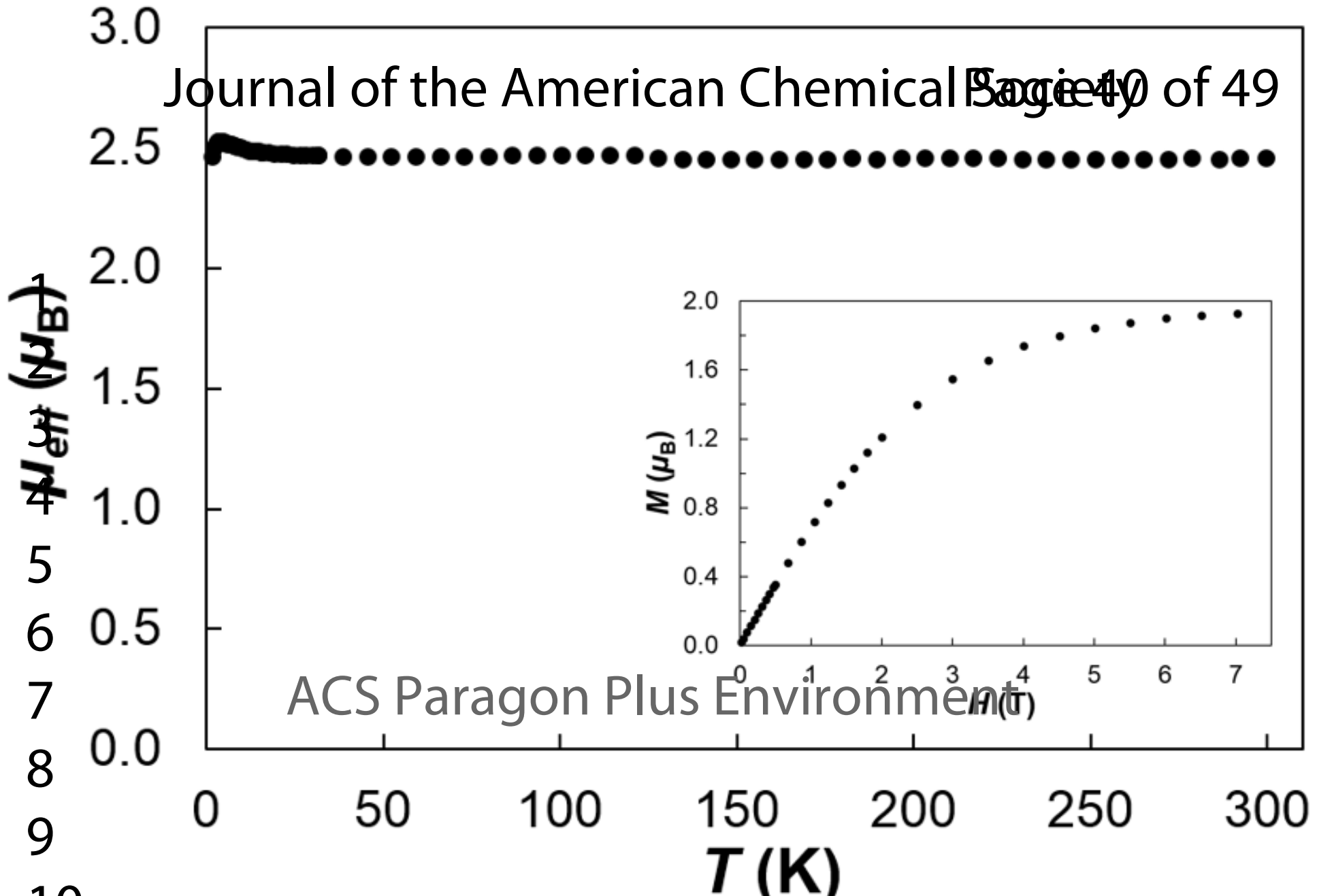

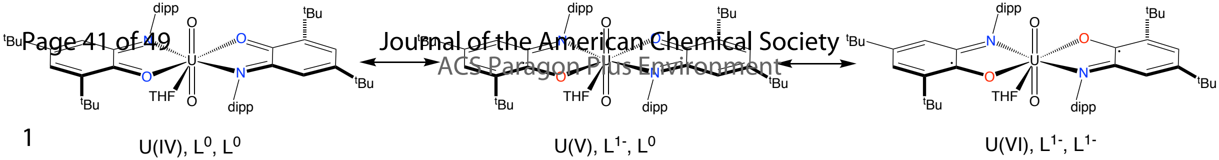
1
U(IV), L0, L0
U(V), L1-, L0
U(VI), L1-, L1-

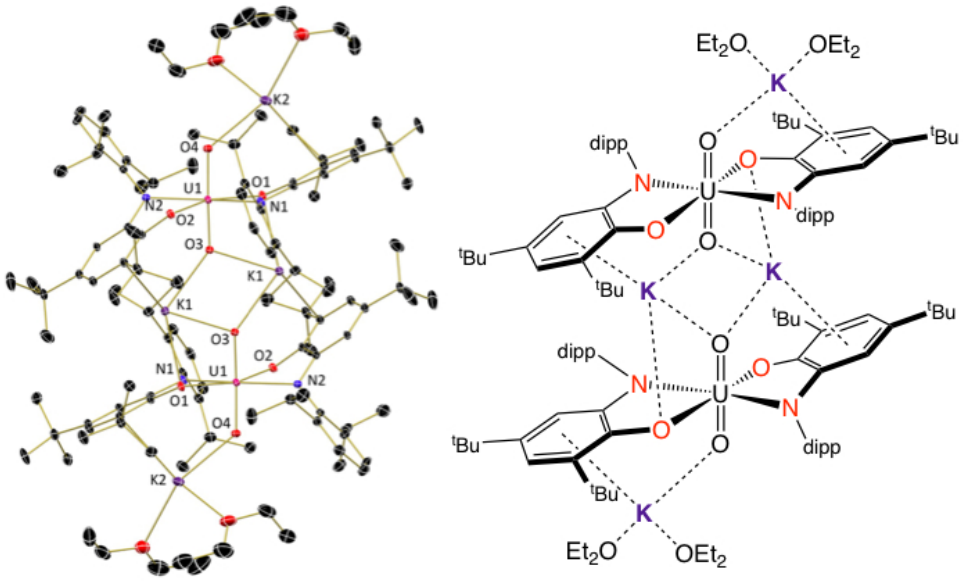

Figure 6. Molecular structure of 3-ap (left) shown with 30% probability ellipsoids. Co-crystallized solvent molecules and H atoms are omitted for clarity. Schematic representation of 3-ap (right), with interactions between potassium ions and various parts of the molecule shown as dashed lines.

914x762mm (20 x 20 DPI)

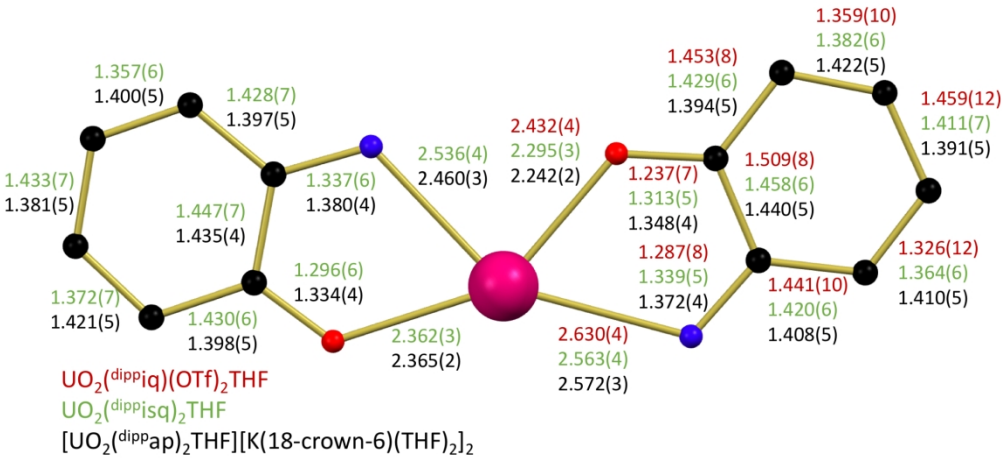

Figure 7. Bond distance comparison (Å) for 1-iq, 2-isq, and 3-ap crown. Carbon atoms shown in black, nitrogen atoms shown in blue, oxygen atoms shown in red, and uranium atom shown in magenta.

921x460mm (62 x 62 DPI)

$UO_2(^{dipp}iq)\ (^{dipp}isq)THFCl$

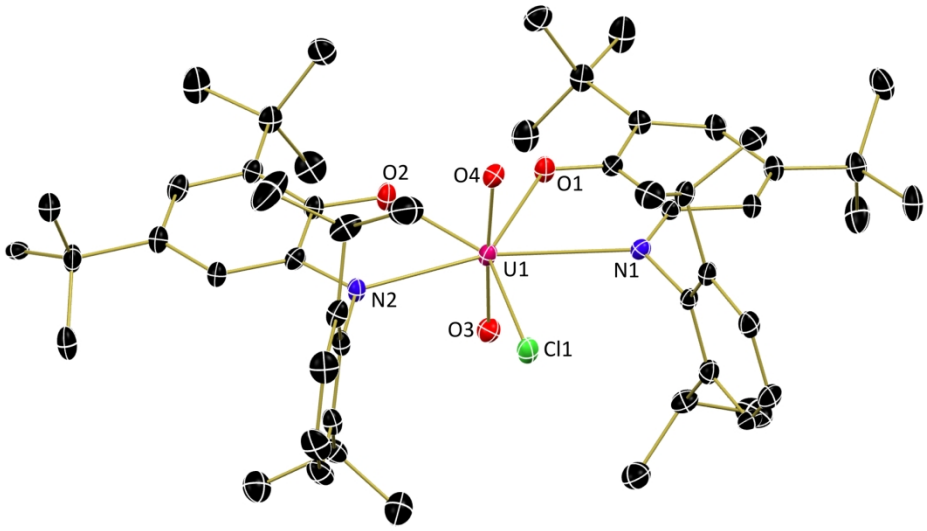

Figure 8. Molecular structure of 4-iq/isq shown with 30% probability ellipsoids. Co-crystallized solvent molecules and H atoms are omitted for clarity.

1057x881mm (72 x 72 DPI)

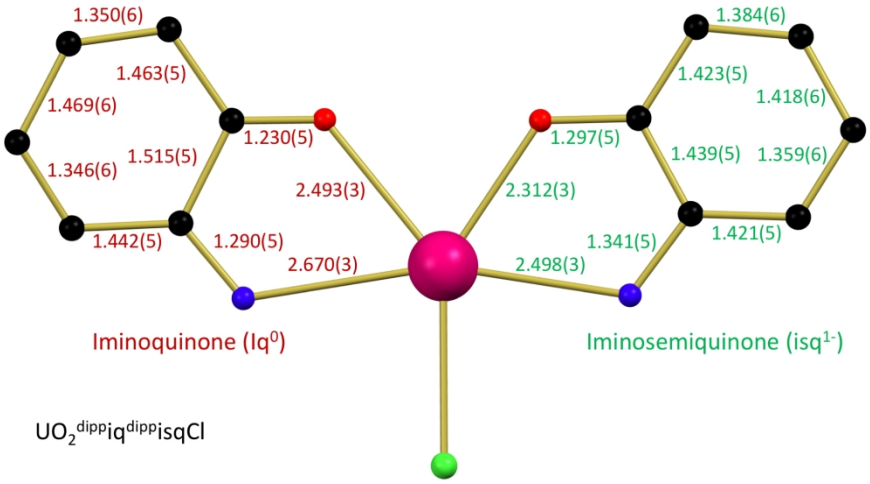

Figure 9. Bond distance comparison (Å) for 4-iq/isq. Carbon atoms shown in black, nitrogen atoms shown in blue, oxygen atoms shown in red, chloride atoms shown in green and uranium atom shown in magenta.

921x460mm (62 x 62 DPI)

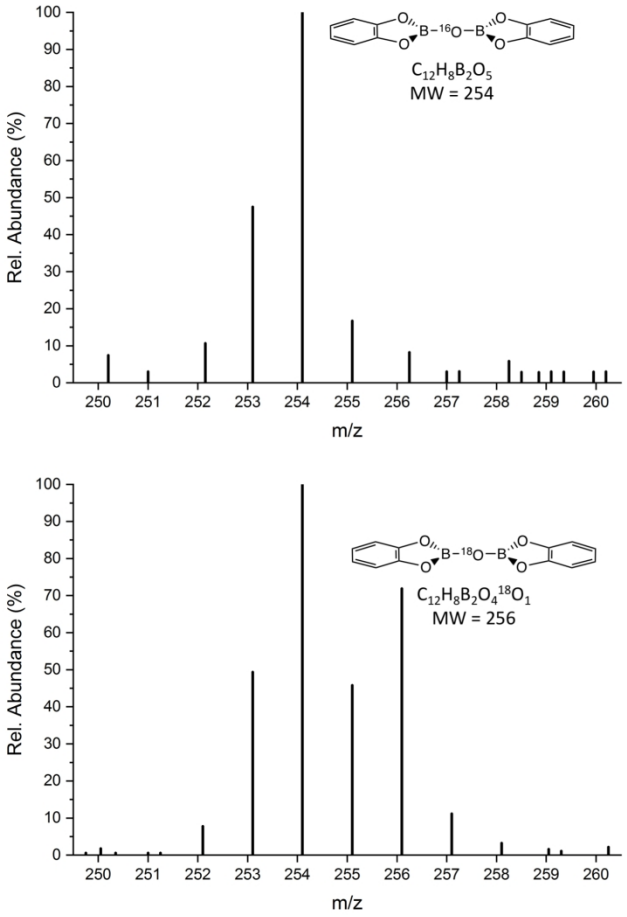

Figure 10. Electron ionization mass spectra (EI-MS) of BOBCat2 from the reaction mixture of ClBCat and 2-isq (top) and 2-isq18 (bottom).

793x793mm (72 x 72 DPI)

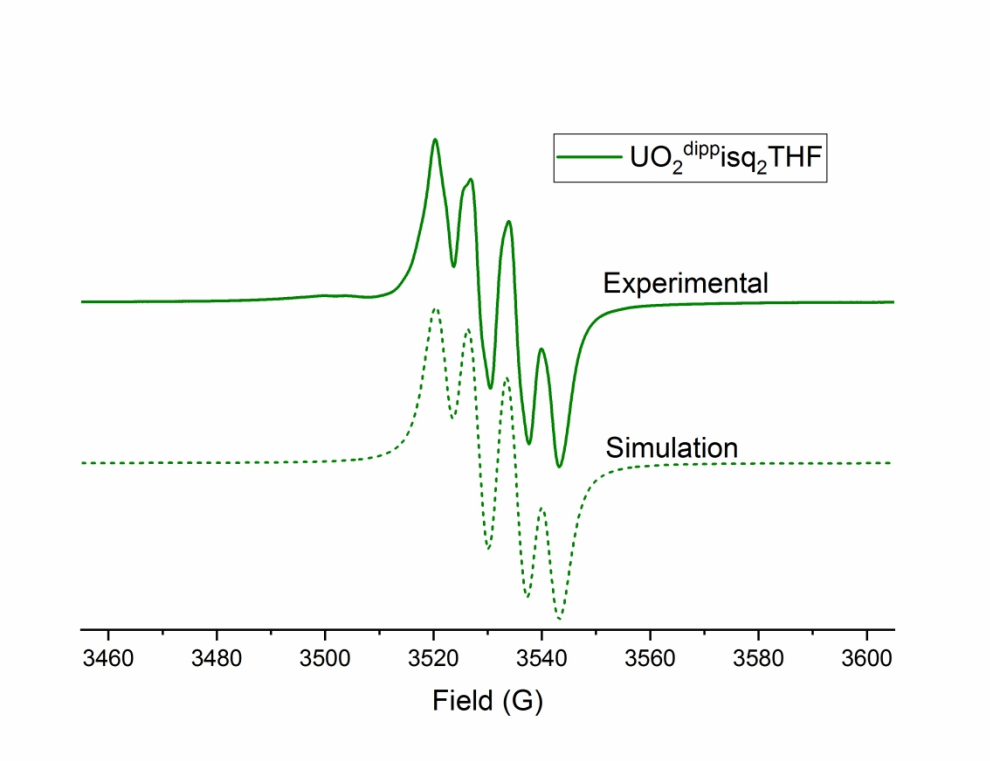

Figure 3. EPR spectrum of 2-isq (n-pentane, 5.8 mM) recorded at 25 °C. giso = 1.993. Frequency: 9.852 GHz. Power: 10 mW. Modulation: 0.5 G/100 kHz.

272x208mm (300 x 300 DPI)

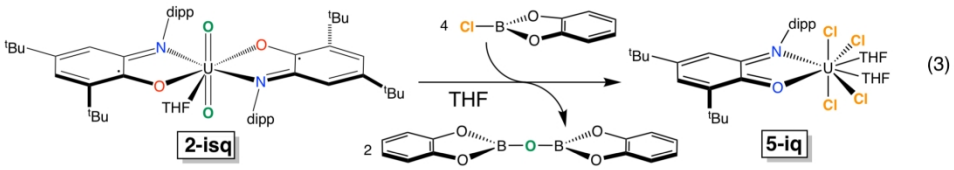

(3)

Equation 3

634x634mm (90 x 90 DPI)

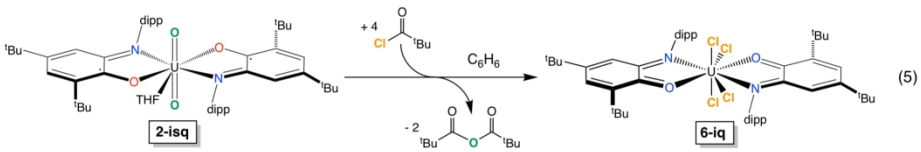

(5)

Equation 5

634x634mm (90 x 90 DPI)